Supporting Information

10.1073/pnas.0902455106

SI Methods

Visual Stimuli. The stimulus array comprised 12 Ts with 4 orientations (up, down, left, or right) arranged in an annulus of 5° radius and displayed across the 4 visual quadrants. The inverted T was the trained target shape, while differently oriented Ts were the distracters. Visual stimuli were generated with a personal computer running in-house software, projected on a NEC 75 F Multisync monitor during behavioral training, and back projected to a translucent screen by an LCD video projector (NEC 830 G+) and viewed through a mirror attached to the head coil during fMRI. Presentation timing was triggered by the acquisition of fMRI frames.

Behavioral Training. Subjects were trained with daily sessions to attend to the lower left visual quadrant and find the target shape among the distracters while maintaining central fixation. Eye position was monitored by eye tracking (ISCN ETL-400 System) to ensure that subjects maintained fixation (see Fig. S1 for representative data from 1 session). Each trial began with a central fixation spot, at which location a cue for the target shape was presented for 2,000 ms, followed by presentation of the stimulus array for 150 ms. The target shape appeared randomly in 1 of 3 possible locations in the lower left visual quadrant, whereas the distracters, changing orientation randomly on each trial, where displayed in all 4 visual quadrants. The task was to indicate the presence or absence of the target by pressing the corresponding button (Cedrus button box), while maintaining fixation on the central spot. Participants performed blocks of 45 trials, 36 (80%) that contained the target and 9 (20%) that did not. Training lasted from 2 to 9 days and continued until the level of performance was >80% in at least 10 consecutive blocks. When the learning threshold was reached, a subset of 6 participants was tested in psychophysics control conditions. They performed the same task but alternated separate blocks of trained/untrained shapes in trained/untrained visual quadrants, giving 8 psychophysical conditions (2 shapes × 4 quadrants).

fMRI Procedure and Scanning. Before behavioral training, imaging data were acquired in a scanning session consisting of 6 runs of resting state, in which subjects were instructed to fixate a small cross under low-level illumination and to remain passive (free from pursuing focused thought), and 6 runs of a functional retinotopic localizer to identify voxels preferentially responding to each of the 4 visual quadrants. We stimulated each visual quadrant independently. Every run consisted of 20 blocks: 16 stimulation blocks (4 for each visual quadrant) in which an array of 3 Ts was flashed at 6.67 Hz for 13 s, randomly interspersed with 4 fixation blocks. When subjects reached the learning threshold, a second functional session was acquired with 6 resting state runs and 6 runs on the trained shape identification task, each consisting of 5 trained and 5 untrained blocks alternated with 5 fixation blocks. In trained blocks, the target was the trained orientation; whereas in untrained blocks the target was an untrained (left or right) orientation. In both cases, the target was presented randomly in 1 of 3 positions in the (trained) lower left visual quadrant. Each block consisted of a cue of the target orientation at central fixation for 2.163 s, followed by 6 consecutive trials similar to training trials (12 s duration). The target was present in 80% (5) of the trials. Fixation blocks lasted randomly 6, 10, or 12 s with equal probability. In both scanning sessions, data were collected using a 1.5 T Siemens Vision scanner. Anatomical images were acquired using a sagittal magnetization-prepared rapid acquisition gradient echo T1-weighted sequence (MPRAGE) with time of repetition (TR) = 9.7 s; echo time (TE) = 4 ms; flip angle (FA) = 12°; time for inversion = 1,200 ms; voxel size = 1 × 1 × 1.25 mm. Functional images were acquired with a gradient echo sequence (TR = 2.163 s; TE = 50 ms; FA = 90; slice thickness = 8 mm) in the axial plane (matrix = 64 × 64, field of view = 240 mm, 3.75 × 3.75 mm in-plane resolution). Sixteen slices were acquired for whole-brain coverage. Resting state runs included 128 frames (volumes), localizer runs 117, and task runs 113.

fMRI Data Preprocessing. Functional data were realigned within and across scanning runs to correct for head motion using an 8-parameter (rigid body plus in-plane stretch) cross-modal registration. Differences in the acquisition time of each slice within a frame were compensated for by sync interpolation. A whole-brain normalization factor was applied to each run to correct for changes in signal intensity between runs (mode of 1,000). For each subject, an atlas transformation (1) was computed on the basis of an average of the first frame of each functional run and MPRAGE structural images to the atlas representative target using a 12 parameter general affine transformation. Functional data were interpolated to 3-mm cubic voxels in atlas space. The atlas representative MPRAGE target brain (711–2C) was produced by mutual coregistration (12 parameter affine transformations) of images obtained in 12 normal subjects (2). All preprocessing steps were performed using in-house software.

Behavioral Analysis. For each block, we recorded the number of positive responses (p) and the reaction time (RT). We then calculated the false-positive rate (fp) (i.e., trials in which the response indicated that the target was seen although the target was absent) for each individual subject. Finally, the value of p was weighted by the value of fp using the formula: $p' = (p - fp)/(1 - fp)$ (3). The false-positive rate was <5% for all subjects. Values were obtained for training, control psychophysics, and task performance in the scanner. Learning measures were computed for each subject for RT and percent of correct responses (accuracy) by subtracting performance on blocks of untrained versus trained (for RT) and trained versus untrained (for accuracy) orientations.

Localizer and Shape Identification Task Data Processing. The BOLD time course at each voxel, for each subject, was subjected to a general linear model with an assumed response function (Boynton hemodynamic model) (4) using in-house software. Constant and linear terms over each BOLD run accounted for baseline and linear drift. Separate functional regressors coded for each of the event types [Localizer: 5 (fixation, lower left quadrant, lower right quadrant, upper left quadrant, and upper right quadrant); Shape Identification Task: 3 (fixation, trained shape, untrained shape)]. A "residuals" dataset was created by summing the modeled responses (but not the constant or linear drift) with the residuals unaccounted for by the linear model. Therefore, this dataset contains the original time series minus the constant and linear drift terms. Group analyses were conducted using voxel-wise random-effect ANOVAs (*t tests*). Statistical images were Monte-Carlo corrected for multiple comparisons over the entire brain ($P < 0.05$), to obtain *z*-score maps. Contrast maps were computed by subtracting ANOVA effects at each voxel to create *z*-score images from a given general linear model. For the Localizer, voxels responding preferentially to

each visual quadrant were found by contrasting the *z*-score image for the desired visual quadrant with the average of the *z*-score images from the other quadrants.

Additional Preprocessing for Resting State Data. In preparation for functional connectivity analysis, data were passed through several additional preprocessing steps: (*i*) spatial smoothing (6 mm full width at half maximum Gaussian blur), (*ii*) temporal filtering retaining frequencies in the 0.009 to 0.08 Hz band, and (*iii*) removal of several sources of spurious variance unlikely to reflect spatially-specific functional correlations through linear regression: (*a*) 6 parameters obtained by rigid body correction of head motion, (*b*) the whole-brain signal averaged over a fixed region in atlas space, (*c*) signal from a ventricular region of interest, and (*d*) signal from a region centered in the white matter.

Control Analyses for fcMRI Change. To confirm that functional connectivity changes reflected prior visual experience, we examined before and after learning changes with an auditory network defined from prior activation studies (5). Aside from scattered correlation differences between individual pairs of regions, there were no systematic learning-dependent changes between auditory regions and dorsal attention or default networks (Fig. S5*A*).

We also investigated whether topographically specific changes of functional connectivity occurred with other task-related networks. Anterior insula and anterior cingulate cortex were recruited by the task (Fig. 3*A*), and are linked at rest in a "task control" network (6). Regions in the motor system were also driven by the response-key press, and form a separate resting-state network. We used motor ROIs obtained in a group of 12 healthy subjects during resting state scans from seeds obtained in a meta-analysis of 2 task-activation motor studies involving right hand pointing movements to a visual target, relative to a control condition in which subjects covertly detected the target (7, 8). The most consistent regions showing high temporal correlation of the spontaneous BOLD signal include bilateral somato-motor cortex, SMA, SII, putamen, thalamus, and cerebellum. The fcMRI motor maps are highly consistent across subjects, with very high *z*-scores, and significantly overlap with task activation maps from the motor activation studies (see Table S3 for a list of ROIs used).

Functional connectivity analysis of seed ROIs in the control and motor network with the visual cortex revealed limited but significant changes postlearning that again involved a trained visual cortex or its homologue in the contralateral hemisphere (Fig. S5*B*).

Finally, we were concerned that functional connectivity changes might reflect covert rehearsal of the task as the second rest scan was acquired shortly after measuring task-evoked modulations. We performed a separate analysis comparing before and after correlation differences separately for the first half [scans 1–3, 15–30 min after performing the task (mean 16 min)] or second half [scans 4–6, 30–45 min later (mean 41 min)] of the postlearning resting state fMRI session. If rehearsal were the explanation for the observed fcMRI changes, one would predict stronger modulations in the first compared to the second half of the after task rest. However, we found the opposite pattern of results, with more robust changes as more time elapsed from the completion of task performance (Fig. S5*C*).

1. Talairach J, Tournoux P (1988) *Co-Planar Stereotaxic Atlas of the Human Brain*. (Thieme Medical Publishers, New York).
2. Snyder AZ (1995) Difference image vs. ratio error function forms in PET-PET realignment. In *Quantification of brain function using PET*, eds Myer R, Cunningham VJ, Bailey DL, Jones T. (Academic, San Diego, CA).
3. Sigman M, Gilbert CD (2000) Learning to find a shape. *Nat Neurosci* 3:264–269.
4. Boynton GM, Engel SA, Glover GH, Heeger DJ (1996) Linear systems analysis of functional magnetic resonance imaging in human V1. *J Neurosci* 16:4207–4221.
5. Belin P, Zatorre RJ, Lafaille P, Ahad P, Pike B (2000) Voice sensitive areas in human auditory cortex. *Nature* 403:309–312.
6. Dosenbach NU, et al. (2007) Distinct brain networks for adaptive and stable task control in humans. *Proc Natl Sci Acad* 104:11073–11078.
7. Astafiev SV, et al. (2003) Functional organization of human intraparietal and frontal cortex for attending, looking, and pointing. *J Neurosci* 23:4689–4699.
8. Astafiev SV, Stanley CM, Shulman GL, Corbetta M (2004) Extrastriate body area in human occipital cortex responds to the performance of motor actions. *Nat Neurosci* 7:542–548.

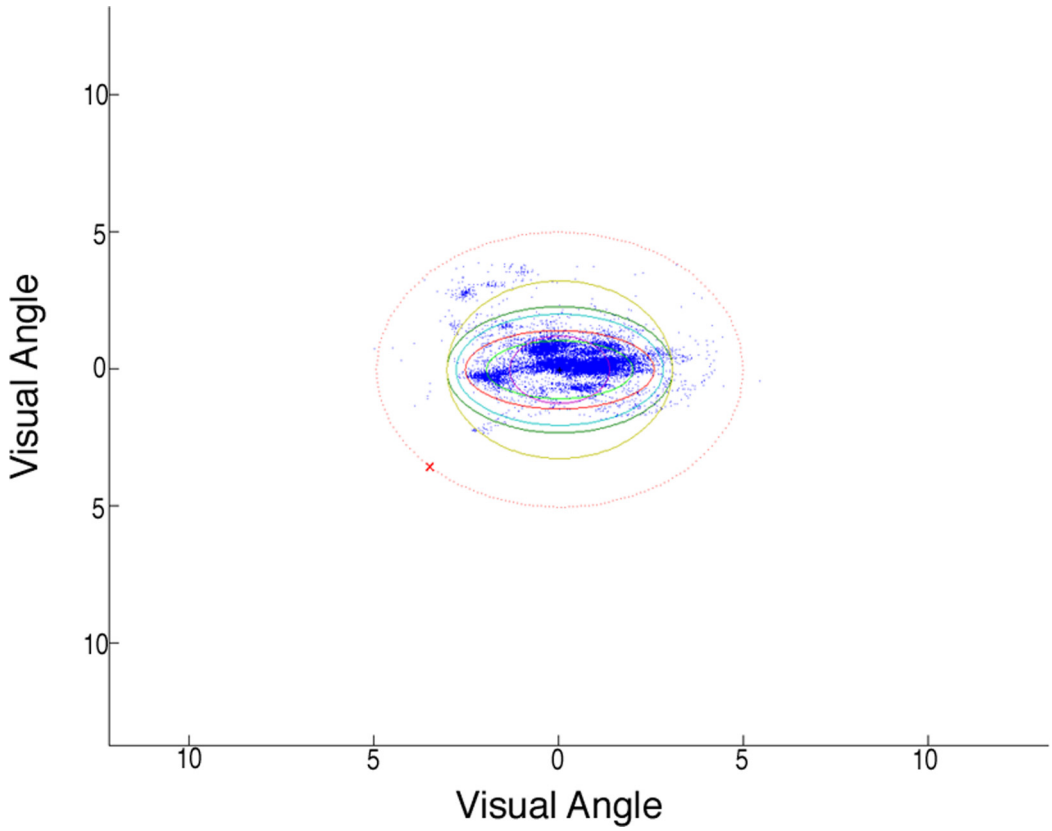

Fig. S1. Eye tracking during behavioral training: Eye position is displayed in screen coordinates, and axes show degree of visual angle from fixation (*Center*). Data are shown from the final training session in a single, representative subject, and is accompanied by ovals showing the standard error from fixation for 6 other subjects in their last or second-to-last training session. Subjects maintained fixation with no systematic deviation toward the attended quadrant.

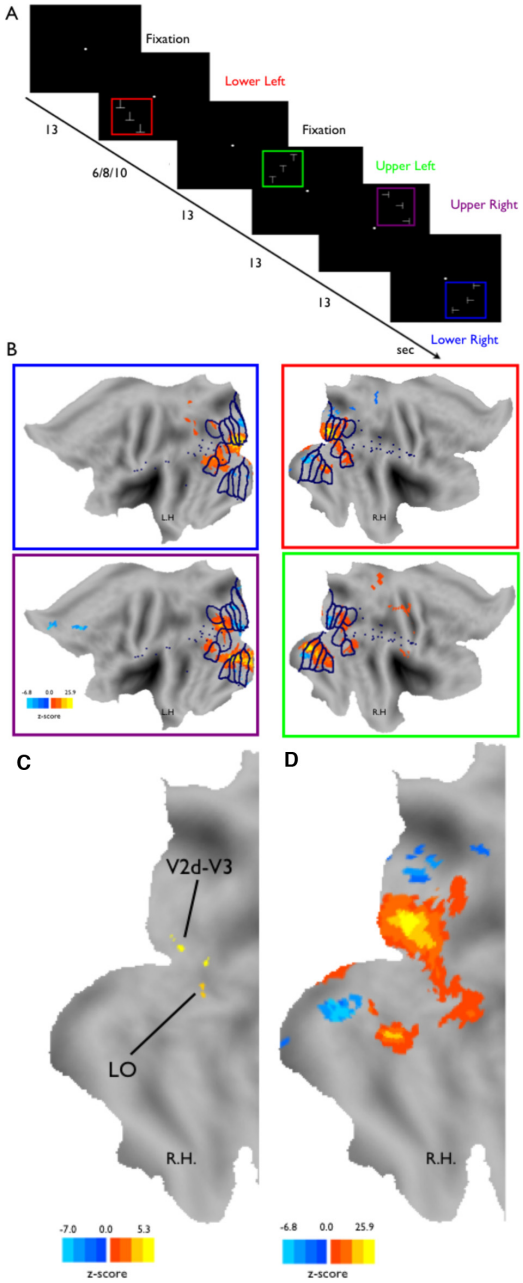

Fig. S2. Functional localizer experiment and comparison of whole-brain voxel-wise modulation after perceptual learning vs. retinotopic localizer. (*A*) Experimental paradigm showing stimulation display and blocked design for stimulation (see *Methods*). Colored square frames mark the 4 visual quadrants (lower left, lower right, upper left, upper right), but were not present in the actual display. Each visual quadrant was separately mapped in a passive stimulation paradigm by flashing one-quarter of the circular stimulus array of Ts. Each run consisted of 20 randomly alternating blocks: 4 for each visual quadrant and 4 fixation blocks. In each stimulation block the stimulus array was flashed at 6.67 Hz for 13 s. Six runs were collected in each subject. (*B*) Flattened brain representation of the PALS (population-average, landmark, and surface-based) atlas (1) with retinotopic borders (blue lines) based on a standard atlas (2). L.H., left hemisphere; R.H., right hemisphere. Voxel-wise group ($n = 12$) activation z-maps are corrected for multiple comparison (Monte-Carlo, $P < 0.05$) over the whole brain. Each colored inset shows the hemisphere contralateral to the stimulated quadrant, and retinotopic selective visual responses obtained by a contrast between the stimulated quadrant minus the average of the other quadrants (see *Methods*). Lower quadrant stimulation (*Left*, *red Inset*; *Right*, *blue Inset*) produce controlateral dorsal responses in V1d, V2d, V3, V3A, V7, LO, and MT+. Upper quadrant stimulation (*Left*, *violet Inset*; *Right*, *green Inset*) activate V1v, V2v, VP, V4v, and V8, but also dorsal responses in V3 to V7, LO, and MT+. (*C*) Voxel-wise z-map corrected for multiple comparisons (Monte Carlo, $P < 0.05$) over the whole brain for trained vs. untrained shape in fMRI experiment projected onto a flattened representation of the PALS atlas (1). Note that voxels responding more strongly to trained than untrained shapes are located in the dorsal visual cortex in V2d/V3 and in LO, and overlap with (*D*) voxels preferentially activated for lower left visual quadrant stimulation. R.H., right hemisphere; LO, lateral occipital; ($n = 12$).

1. Van Essen DC (2005) A population-average, landmark- and surface-based (PALS) atlas of human cerebral cortex. *NeuroImage* 28:635–662.
2. Van Essen DC (2002) Windows on the brain: The emerging role of atlases and databases in neuroscience. *Curr Opin Neurobiol* 12:574–579.

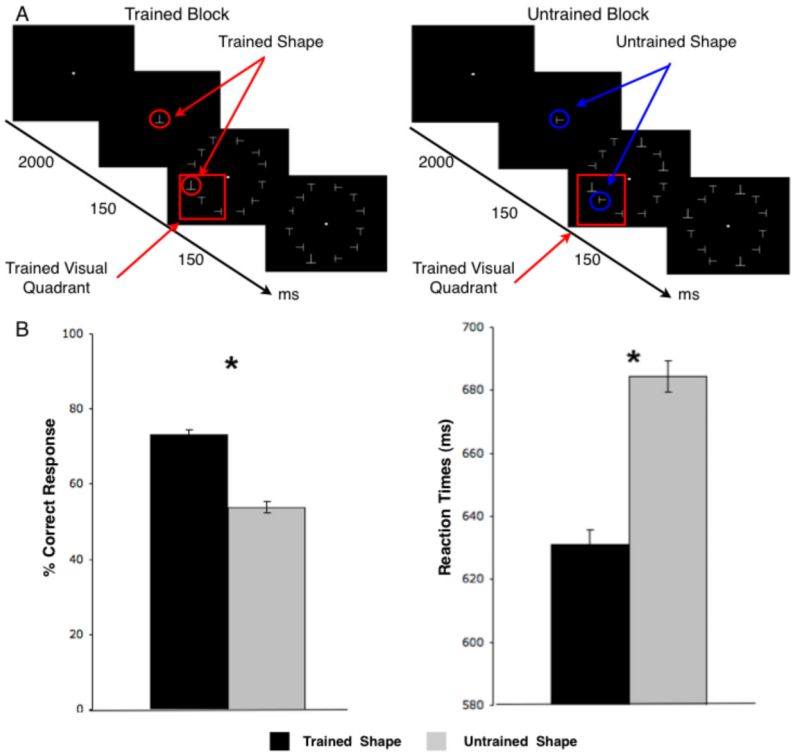

Fig. S3. Task-related activity and psychophysics: paradigm (*A*) and results (*B*) inside the scanner. (*A*) Time line for 2 trials in trained (*Left*) and untrained (*Right*) condition (see *Methods*). Red frame indicates trained visual quadrant, red circle indicates trained shape, and blue circle indicates untrained shape. Colored frame and circles were not displayed on the monitor. After training and reaching criterion, subjects were scanned in a blocked design to study modulations of task-evoked activity. Six scans consisting of randomly alternating blocks of trained (attend to trained visual quadrant, detect trained shape), untrained (attend to trained visual quadrant, detect untrained shape), or fixation were run. On trained blocks, the target was the trained orientation presented randomly in 1 of 3 positions in the trained quadrant, whereas in untrained blocks, the target was an untrained (left and right) orientation. Each block consisted of a central cue indicating the target orientation for that block of trials for 2.163 s, followed by 6 trials in sequence for a duration of 12 s. The target was present on 80% of the trials. Fixation blocks lasted randomly 6, 10, or 12 s with equal probability. (*B*) Behavioral results inside the scanner. (*Left*) Accuracy (% correct response) on blocks of trials with trained (*black*) vs. untrained (*gray*) shape. (*Right*) Reaction times (ms) of correct response ($n = 14$); Student's t test, *, $P < 0.01$; error bars represent SEM. Note orientation-specific learning effect such that performance in the trained quadrant is higher for trained as compared to untrained shape.

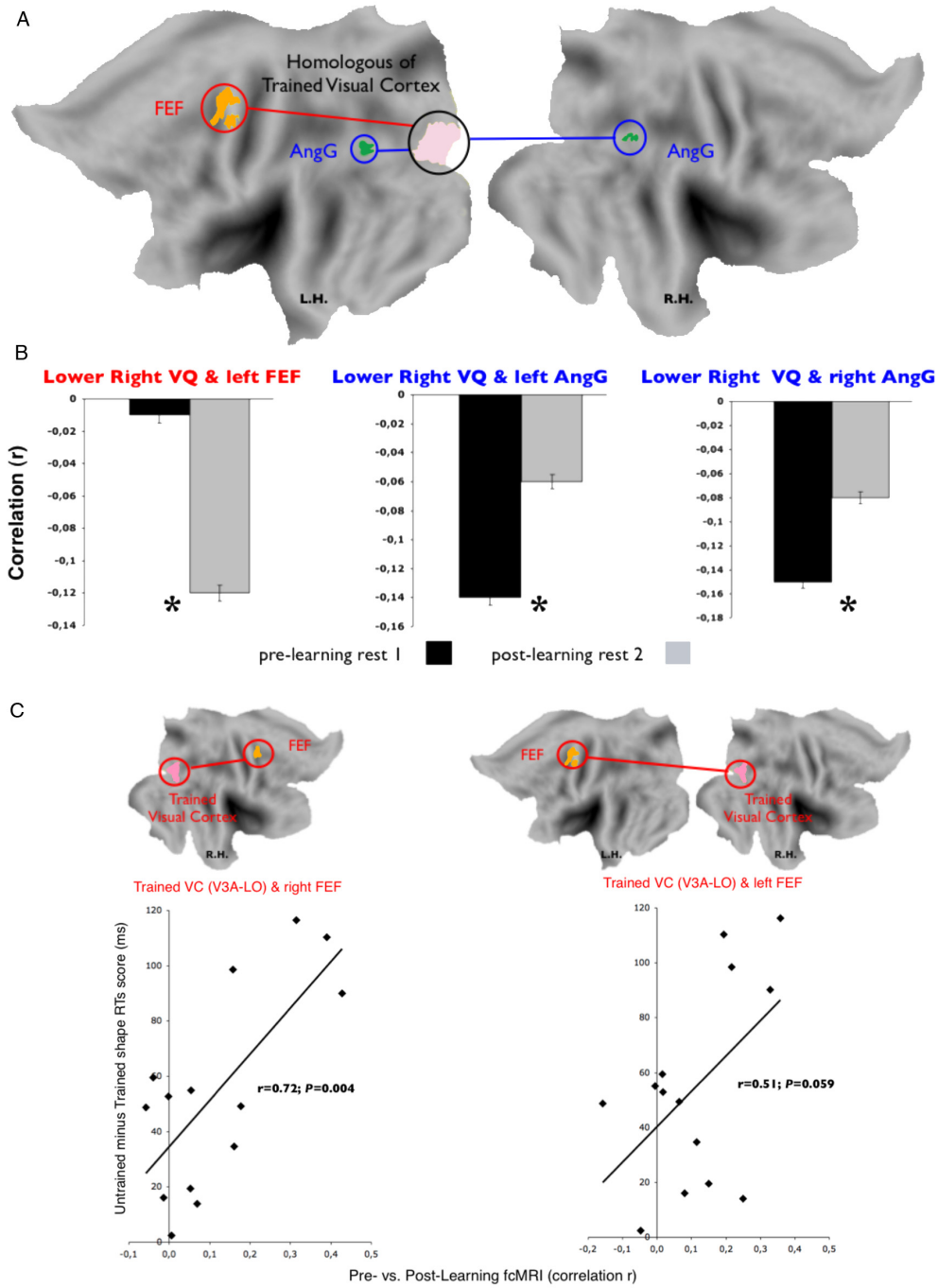

Fig. S4. Modulation of fcMRI in left dorsal visual cortex, corresponding to right lower quadrant homologous to trained left lower quadrant and correlation between fcMRI changes and behavioral performance. (*A*) ROIs in lower right visual quadrant, homologous to trained visual cortex, left FEF (DAN) [Corbetta M, Shulman GL (2002) Control of goal-directed and stimulus-driven attention in the brain. *Nat Rev Neurosci* 3:201–215], and left/right AngG (DMN) [Shulman GL, et al. (1997) Common blood flow changes across visual tasks: II. Decreases in cerebral cortex. *J Cognit Neurosci*, 9:648–663]. (*B*) Correlation values (*r*) between right visual quadrant and left FEF, left/right AngG ROIs (*Left*, *Center*, and *Right*, respectively) before (*black*) and after (*gray*) learning. AngG, angular gyrus; FEF, frontal eye field; L.H., left hemisphere; R.H., right hemisphere; VQ, visual quadrant; ($n = 14$); *r*, Pearson correlation coefficient; Student's *t test*, 2 tails, $P < 0.05$; error bars represent SEM. Note that that the right lower quadrant shows modulations that are similar to those observed in the trained cortex (*Left*) (i.e., more negative modulation with DAN) and in the untrained cortex (*Right*) (i.e., less negative modulation with DMN). (*C*) Scatter plots between fcMRI correlation differences before and after learning (*x*-axis), and behavioral differences (reaction times) between untrained and trained shape blocks in the scanner (*y*-axis). Each diamond represents a single subject (right FEF-trained visual cortex, $r = 0.72$, $P = 0.0038$; left FEF-trained visual cortex, $r = 0.51$, $P = 0.059$). LO, lateral occipital; VC, visual cortex. ($n = 14$).

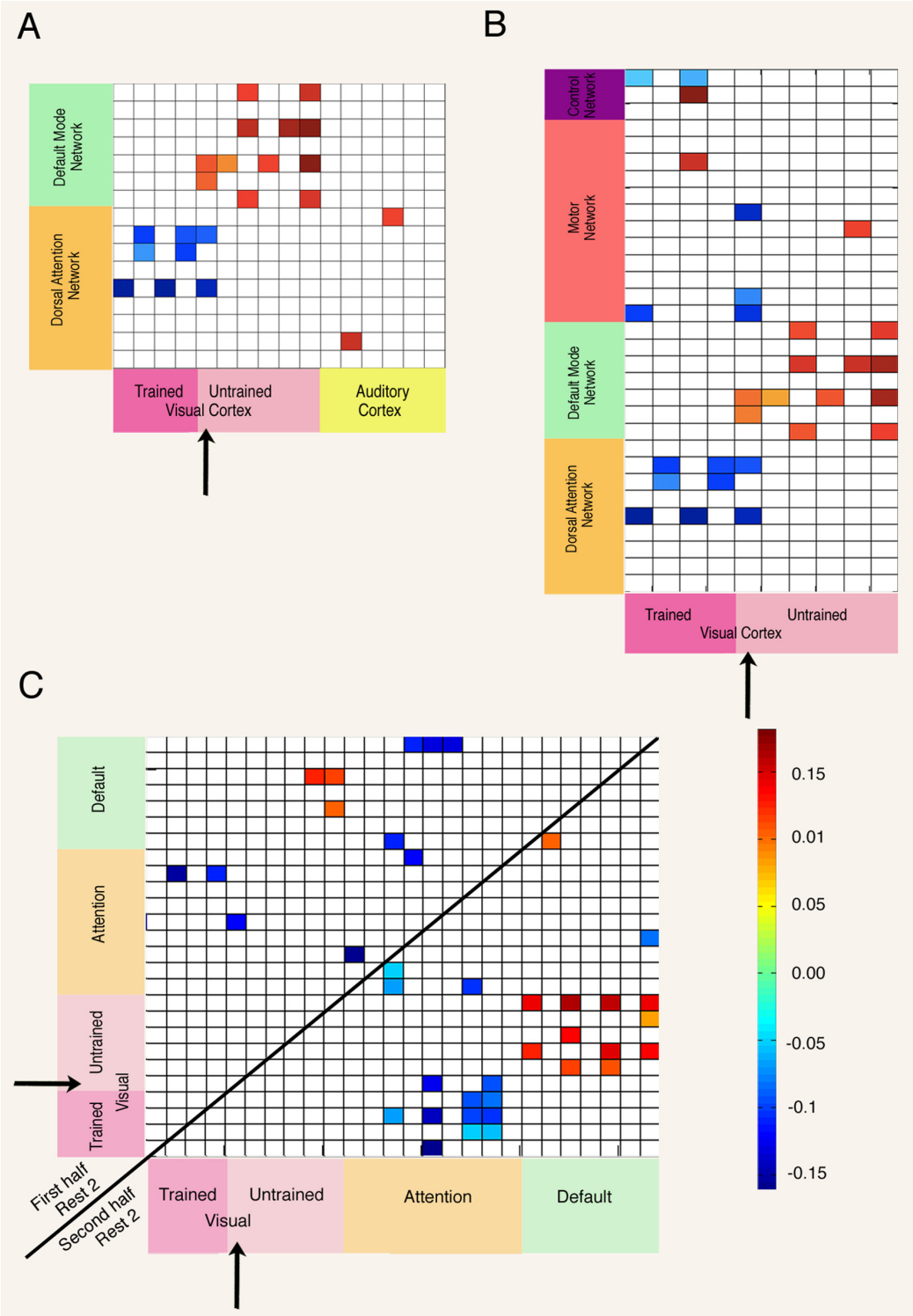

Fig. S5. Control analyses for fcMRI change. Analysis performed to assess the specificity of learning induced fcMRI changes. (*A*) Correlation changes found between ROIs in the visual and auditory cortex and the dorsal attention and default mode networks. The auditory cortex shows no systematic modulation in fcMRI by learning. All differences were computed on Fisher *z*-transformed correlation coefficients. (*B*) Correlation changes found between ROIs in the task-related motor and control networks show topographic specificity for the trained visual quadrant. (*C*) Correlation changes separately computed on the first and second half of the postlearning rest to ensure that modulation was not a result of covert task rehearsal. Top half shows the changes in the first half of postlearning rest and the bottom-half shows those that occurred in the second portion. The black arrow denotes early portions of left dorsal visual cortex homologues to trained visual cortex and shows both sets of fcMRI modulations.

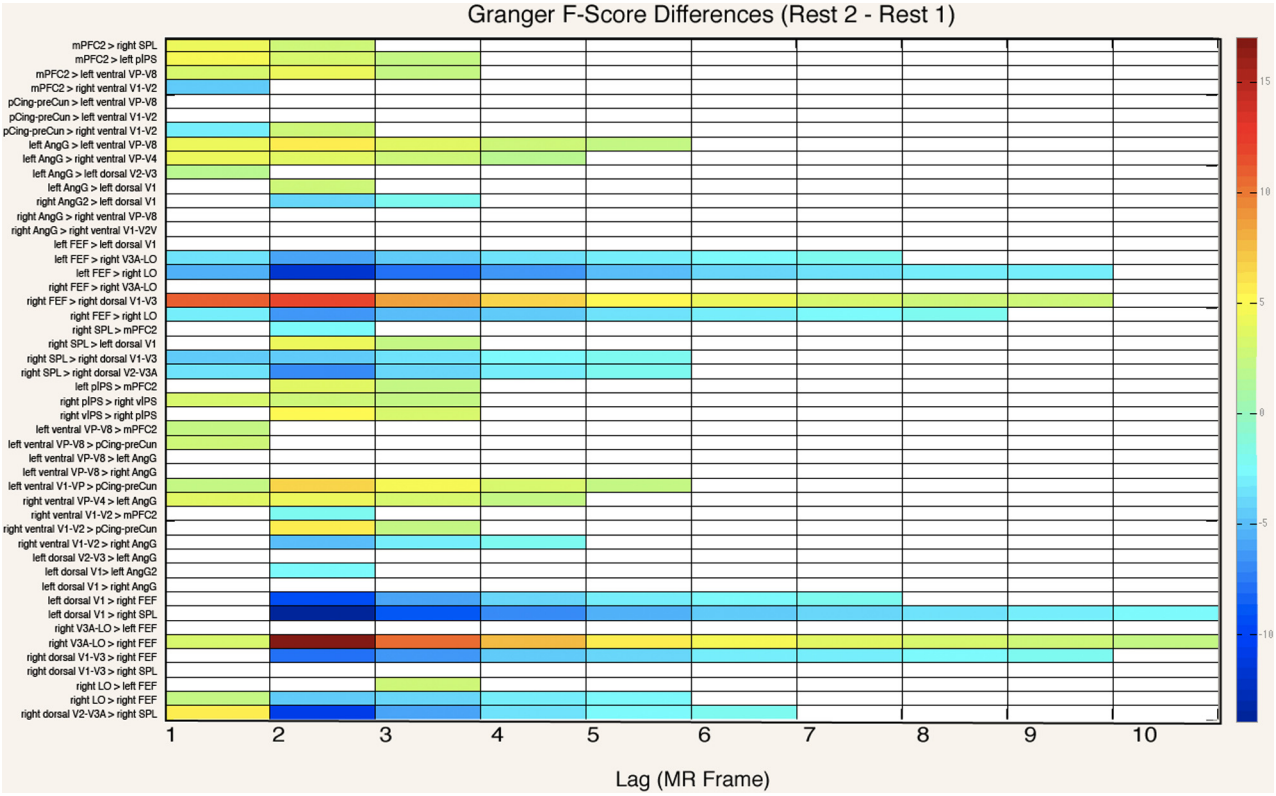

Fig. S6. GC analysis. *x*-axis: ROI pairs between visual, DAN, DMN networks. (*Top*) Top-down direction (e.g., right FEF-to-right V3A); (*Bottom*) Bottom-up direction (e.g., right V3A-to-right FEF). *y*-axis: lag or MR frame over which GC was calculated. Color scale is Granger F-score, indicating how significantly estimates of a region time course improve by adding information from another region's time course. For example, how information about the variance in V3A time series is improved by adding information from the time-series of FEF. This calculation is performed at different lags, which indicate how much earlier in time this relationship holds.

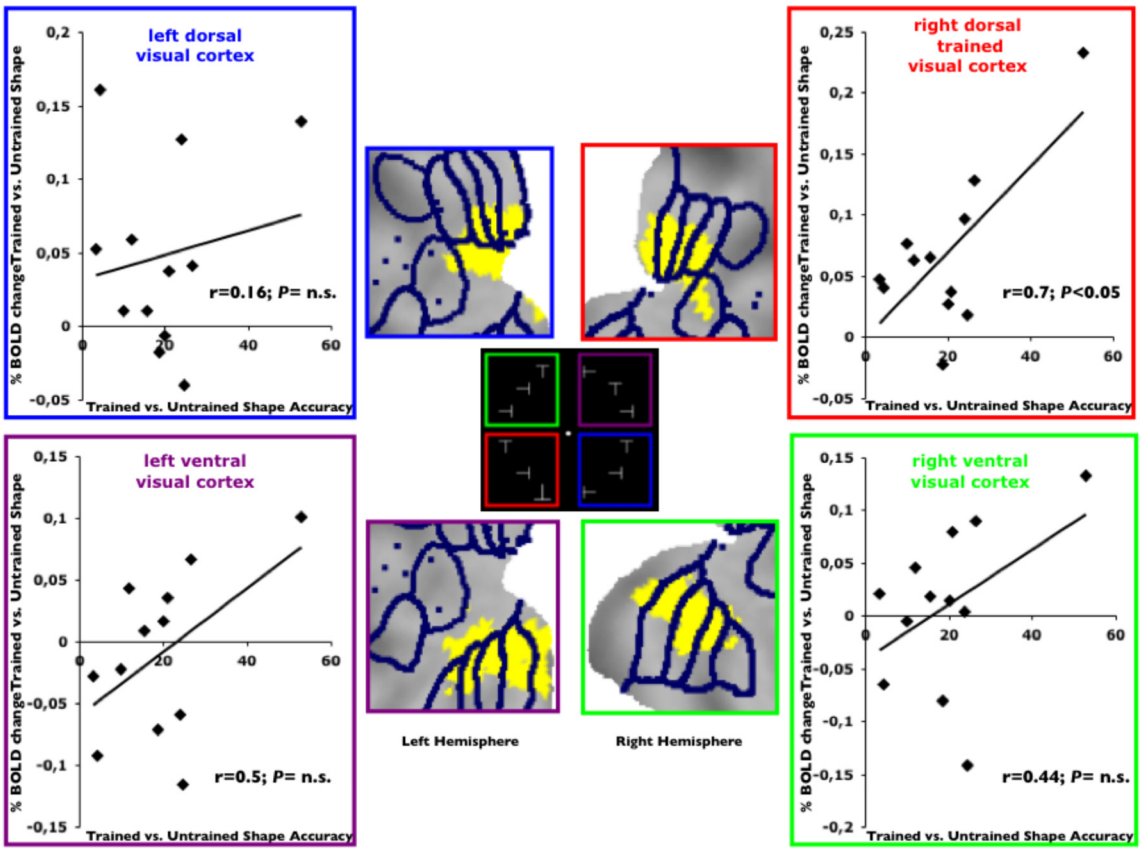

Fig. S7. Correlation between task-evoked BOLD signal modulation in the visual cortex and behavioral performance. Behavioral improvement, as measured by trained minus untrained shape accuracy, positively correlates with BOLD signal change between trained vs. untrained shape. (*Center*) Stimulus array with colored squares (not present in real display) indicating 4 visual quadrants. (*Flat maps*) Visual cortex ROIs obtained from passive localizer scans by stimulating 1 quadrant at a time (see Fig. S1). ROIs are projected onto a flattened representation of posterior occipital cortex using the PALS atlas [Van Essen DC (2005) A population-average, landmark- and surface-based (PALS) atlas of human cerebral cortex. *NeuroImage* 28:635–662]. Blue lines are approximate borders between retinotopic visual areas based on a standard atlas [Van Essen DC (2002) Windows on the brain: The emerging role of atlases and databases in neuroscience. *Curr Opin Neurobiol* 12:574–579]. Scatter plots show the correlation between accuracy score (*x*-axis) and % BOLD change (*y*-axis) in trained vs. untrained condition; each diamond represents one subject ($r = 0.7$, $P = 0.006$ for *Lower Left*; $r = 0.27$, $P = 0.38$ for *Lower Right*; $r = 0.45$, $P = 0.143$ for *Upper Left*; $r = 0.42$, $P > 0.17$ for *Upper Right*); *r*, Pearson coefficient; $n = 12$; significant $P < 0.05$.

Table S1. Performance results for individual subjects

	Training				Scanner	
Subjects	Accuracy 10 blocks	Slope 10 blocks	Number of blocks	Slope All blocks	Accuracy T vs. U	RTs U vs. T
Andant	31.8	5.4378	76	1.5658	15.6	59.55
Anndel	47.6	7.8672	135	0.8793	20.8	48.8
Augpel	44.4	6.6424	131	0.9081	18.6	52.79
Crisar	68.6	10.0289	45	2.6922	20	34.74
Fracav	13.11	2.0162	189	0.5283	26.7	13.9
Fracia	61.73	9.5234	109	0.9736	3.4	116.37
Giavil	47.0	7.8732	77	1.572	23.9	49.27
Grabis	41.6	6.6108	75	1.4934	52.7	98.5
Iolpan	53.3	7.8617	160	0.6473	10	54.96
Marvil	19.3	3.2592	161	0.6652	40.1	110.04
Matlav	41.3	5.4611	95	1.0518	11.8	19.5
Micnav	35.1	5.6019	239	0.3947	4.4	16.06
Stebur	20.9	3.4766	144	0.6825	24.5	2.35
Verdei	46.7	7.6348	110	1.0707	26.5	90.08

This table reports behavioral results for each subject during training and inside the scanner. It is clear that a high variability exists across subjects. RTs, reaction times; SD, standard deviation; SE, standard error; T, trained; U, untrained.

Table S2. ROIs functionally defined from the visual localizer (see *Methods*)

Coordinates	Visual quadrant	Visual cortex	Regions	Voxels	z-Score
+14 −92 + 20	Lower left	Right dorsal	V1-V2d-V3	221	25.35
+28 −86 + 11	Lower left	Right dorsal	V3A, LO	138	16.04
−13 −97 + 14	Lower right	Left dorsal	V1-V2	220	19.26
−10 −85 + 01	Lower right	Left dorsal	V3-V3A	104	12.73
+09 −80 −06	Upper left	Right ventral	V1-V2v	201	28.94
+23 −75 −12	Upper left	Right ventral	VP-V4v	249	17.70
−19 −78 −12	Upper right	Left ventral	V1-V2v-VP	214	23.05
−04 −83 −07	Upper right	Left ventral	VP-V4v-V8	163	18.65

For each visual quadrant, we first selected ROIs with z-score $>$ 0, then we took the 2 most significant ROIs.

Table S3. ROIs functionally defined from shape-identification task, as well as those taken from the literature for control analysis (see *Methods*)

Coordinates	Regions	Label	System	Voxels	z-Score
+17 97− + 16	V2d, V3	V2d, V3	Visual	27	4.39
+38 −87 + 07	Lateral occipital	LO	Visual	10	3.87
−37 −78 + 34	Left angular gyrus	LAngG	DMN	73	4.34
−47 −62 + 42	Left angular gyrus 2	LAngG2	DMN	65	4.06
−04 −46 + 32	posterior cingulate/precuneus	pCing-preC	DMN	100	3.88
+53 −61 + 27	Right angular gyrus	RAngG	DMN	25	3.72
+45 −63 + 48	Right angular gyrus 2	RAngG2	DMN	15	3.67
00 + 54 + 01	Left medial prefrontal cortex	LmPFC	DMN	18	3.63
−15 + 52 + 33	Left medial prefrontal cortex 2	LmPFC2	DMN	30	3.42
−14 −69 + 48	Left superior parietal lobule	LSPL	DAN	88	−4.35
+32 −60 + 51	Right posterior intraparietal sulcus	RpIPS	DAN	40	−4.21
+14 −67 + 53	Right superior parietal lobule	RSPL	DAN	103	−4.19
−34 −09 + 53	Left frontal eye fields	LFEF	DAN	109	−3.97
−44 −66 −08	Left middle temporal region	LMT+	DAN	45	−3.91
+30 −04 + 52	Right frontal eye fields	RFEF	DAN	42	−3.85
−25 −72 + 26	Left ventral intraparietal sulcus	LvIPS	DAN	46	−3.80
−29 −60 + 50	Right posterior intraparietal sulcus	LpIPS	DAN	76	−3.80
+43 −09 + 20	Right anterior temporal	RaTemp	Auditory	81	NA
+44 −32 + 16	Right posterior temporal	RpTemp	Auditory	81	NA
+58 −12 + 02	Right temporal	RTemp	Auditory	81	NA
−38 −34 + 12	Left posterior temporal	LpTemp	Auditory	81	NA
−57 −02 + 20	Left temporal	LTemp	Auditory	81	NA
−57 −16 + 01	Left anterior temporal	LaTemp	Auditory	81	NA
+34 + 17 + 02	Reft anterior insula	RaIns	Control	81	NA
−36 + 13 + 01	Left anterior insula	LaIns	Control	81	NA
+04 + 13 + 39	Dorsal anterior cingulate cortex	dACC	Control	81	NA
−18 −51 −24	Left cerebellum	lCbllm	Motor	81	NA
−32 −32 + 52	Left central sulcus	lCS	Motor	81	NA
−29 −17 + 10	Left putamen	lPut	Motor	81	NA
−39 −25 + 18	Left SII	lSII	Motor	81	NA
−01 −14 + 51	Left SMA	lSMA	Motor	81	NA
−13 −25 + 03	Left thalamus	lThal	Motor	81	NA
+15 −50 −20	Right cerebellum	rCbllm	Motor	81	NA
+32 −31 + 55	Right central sulcus	rCS	Motor	81	NA
+30 −16 + 09	Right putamen	rPut	Motor	81	NA
+36 −21 + 20	Right SII	rSII	Motor	81	NA
+04 −12 + 49	Right SMA	rSMA	Motor	81	NA
+14 −25 + 05	Right thalamus	rThal	Motor	81	NA

For each visual quadrant, we first selected ROIs with z-score $>$ 0, then we took the 2 most significant ROIs. DAN, Dorsal Attention Network [Corbetta M, Shulman GL (2002) Control of goal-directed and stimulus-driven attention in the brain. *Nat Rev Neurosci* 3:201–215]; DMN, Default Mode Network [Shulman GL, et al. (1997) Common blood flow changes across visual tasks: II. Decreases in cerebral cortex. *J Cogn Neurosci*, 9:648–663].